




Investigation of the seat-dip effect using finite-difference time-domain simulations

Julie Meyer,^{a)}  Henna Tahvanainen,^{b)}  Jukka Saarelma, and Tapio Lokki 

Acoustics Lab, Department of Information and Communications Engineering, Aalto University, 02150 Espoo, Finland

ABSTRACT:

The seat-dip effect (SDE) occurs when low-frequency sounds propagate through the seating area of a performance space. The physical aspects governing the effect still puzzle acousticians mostly due to the large variety of seating configurations. In this study, the SDE is investigated in three parameterized hall models using the finite-difference time-domain method to simulate a large number of seat configurations in order to quantify the contribution of different geometric properties related to the seating area. The results show that the step size defining the inclination angle of the seating area and the opening underneath the seats (or underpass) are significant factors contributing to the SDE, whereas the stage height and the source position are found to be less important. The results also demonstrate that with an underpass greater than the step size, the first frequency dip occurring between 80 and 100 Hz is mitigated regardless of the hall type considered. The phenomenon is also found to be predominant in the early part of the room response. Visualizations of spatial and time-frequency evolution in the halls are also provided for the cases where the seat properties are found to visibly affect the magnitude spectrum.

© 2023 Acoustical Society of America. <https://doi.org/10.1121/10.0020826>

(Received 26 March 2023; revised 14 July 2023; accepted 8 August 2023; published online 13 September 2023)

[Editor: Siu-Kit Lau]

Pages: 1628–1639

I. INTRODUCTION

One of the low-frequency phenomena occurring in large performance spaces is the seat-dip effect (SDE). The effect can be described as a series of peaks and dips in the frequency response of the space which is formed by sound waves emanating from the stage and traveling at grazing angles over the seating area. As suggested by its name, the main feature of the effect is typically one deep dip between 80 and 300 Hz in the early part of the magnitude of the Fourier-transformed room impulse response, though the influence of the effect can extend up to about 1 kHz (Schultz and Watters, 1964; Sessler and West, 1964). The SDE can be audible in concert halls where late reverberation is at a relatively low level (Tahvanainen *et al.*, 2017). In particular, the geometry of the seats greatly influences the frequency response characteristics, and there is a smaller variation due to source and receiver positions among other parameters (Davies, 1992; Ishida, 1993; Schultz and Watters, 1964; Sessler and West, 1964; Tahvanainen, 2021).

The SDE can be qualitatively predicted by scattering over a periodic structure and considering the seating area as an absorbing layer over a rigid floor (Takahashi, 1997). Other analytical models exist but the results are not fully in line with measurements (Ishida, 1995; Sakurai *et al.*, 1993). Regarding measurements, studying the SDE also comes with a few drawbacks. For example, it is impossible to

quantify the effect of each geometrical property of the seating area on the SDE because many of them simultaneously vary across halls (Tahvanainen *et al.*, 2015a). With scale model measurements, only a subset of these attributes has been considered individually. Furthermore, visualizing the resulting wavefront pattern requires laborious measurements (Witew *et al.*, 2017).

As an alternative to measurements, the SDE has been studied using several wave-based modeling methods such as the boundary element method in Ando *et al.* (1982), Davies and Cox (2000), Kawai and Terai (1991), and Osa *et al.* (2007); the finite element (FE) method in Min and Liao (2021); and finite difference methods in Lokki *et al.* (2011), LoVetri *et al.* (1996), and Lokki *et al.* (2013). The main objectives of these studies have been to analyze and explain the SDE and to devise measures for its elimination while focusing on single source-receiver positions. Among these numerical modeling techniques, the finite-difference time-domain (FDTD) method is of particular interest to simulate the SDE occurring at relatively low frequencies since the largest of the numerical errors associated with the method [usually being the discretization error (Oberkampf and Roy, 2010, p. 286)] increases as a function of frequency. As such, using a numerical modeling method like FDTD enables to directly obtain time-domain responses in three-dimensional domains while limiting the amount of numerical error present in the simulated results. Recently, the FDTD method was employed for large-scale acoustic modeling of concert halls, but the geometry of the seating area was approximated with large blocks (Fratoni *et al.*, 2022). Consequently, there was a considerable discrepancy

^{a)}Current address: Dyson School of Design Engineering, Imperial College London, UK. Electronic mail: jmeyer@ic.ac.uk

^{b)}Current address: Department of Industrial Engineering, University of Bologna, Bologna, Italy.

between the simulation and measurement results at the 250 Hz octave band.

In this paper, three parameterized concert halls with approximate, yet seat-like, periodic structures are simulated using the FDTD method with the aim of (i) understanding how individual seat attributes influence the SDE, (ii) visualizing the effect through spatial analysis of the time-frequency evolution in the investigated hall models (full videos are provided as supplementary material for several parameter conditions and frequencies).¹ Prior to simulating the various concert hall configurations, a mathematical process aiming at quantifying the numerical errors present in the simulated results is conducted.

II. BACKGROUND

A. The SDE

The inauguration of the New York Philharmonic Hall and the subsequent studies on the cause of the perceived lack of bass led to the concept of the low-frequency attenuation called the SDE (Schultz and Watters, 1964; Sessler and West, 1964). Based on measurements by Tahvanainen *et al.* (2015a) in a large number of concert halls, this low-frequency attenuation is characterized either by a deep dip between 80 and 100 Hz or an asymmetric dip between 200 and 300 Hz in the magnitude spectrum at 20 ms after the arrival of the direct sound, so that the frequency of the dip corresponds to about 1/4 wavelength of the seat backrest height (Bradley, 1991; Ishida, 1993). The deep dip is associated with closed seats, where the seat backrest extends to the floor and the asymmetric dip with seats with an underpass referred to as open seats. For stepwise raked floors, the underpass is sometimes entirely blocked by the step, which generally renders the seats closed from the point of view of the SDE. Based on the scale model measurements, the frequency of the dip increases with the size of the underpass (Sessler and West, 1964; Tahvanainen *et al.*, 2020). In addition, there is some indication that the underpass introduces a considerable boost at low frequencies below the main dip (Tahvanainen *et al.*, 2020).

The SDE appears to be a sum of multiple phenomena: destructive and constructive interference, diffraction over periodic roughness, and bending towards an absorptive surface. The direct sound and the reflected sound from the seats interfere destructively at the frequency whose 1/4 wavelength corresponds to the seat backrest height (Ishida, 1993). Generally, sound waves traveling at grazing angles over a rough structure undergo low-frequency attenuation when the roughness is smaller than the acoustic wavelength (Twersky, 1957). In concert halls, such a rough structure is the seating area. Additionally, the sound waves can scatter or diffract on the top of the seat backrests. In addition, surface waves could explain the boost of the level below the main attenuation frequency (Mommertz, 1993). Finally, some resonances/standing waves between the vertical and horizontal spacing between the seats may be involved (Bradley, 1991; Min and Liao, 2021; Sessler and West,

1964). The vertical resonance frequency depends on the seat backrest height and whether the seats are open with an underpass, thus forming a cavity open at both ends (half-wave resonator) or closed at one end (quarter-wave resonator). The horizontal resonance could be formed between the two seating rows, which would account for the secondary dip at a higher frequency in certain seat backrest height and row spacing combinations (Bradley, 1991). An FE-model of closed seats suggests that the main mechanisms of the SDE are standing waves between the seats and diffraction vortices on the tops of the seat backrests (Min and Liao, 2021).

The angle of incidence seems to have an effect on the frequency and amplitude of the main SDE attenuation (Davies, 1992; Ishida, 1993; Schultz and Watters, 1964; Sessler and West, 1964). Typically, the effect forms over several rows of seats and is leveled off with reflections not arriving at grazing angles (Bradley, 1991; Pätynen *et al.*, 2013; Sessler and West, 1964; Tahvanainen *et al.*, 2015a). Finally, most of the studies involving the SDE have been conducted in the absence of an audience as it is a rather special task to run measurements with fully occupied performance spaces. The effect of an audience seems to depend on the seat properties as summarised by Tahvanainen and Lokki (2018). Namely, if the seat underpasses are small, the audience legs may block them and bass boost below the main attenuation may be lost. Furthermore, the frequency of the main attenuation may change according to the relationship between the seat backrest height and the height of the shoulders of the seated audience.

B. The FDTD method

The partial differential equation of interest in room acoustics is the linear wave equation, which in 3-D Cartesian coordinate system is given by

$$\frac{\partial^2 p}{\partial t^2} = c^2 \left(\frac{\partial^2 p}{\partial x^2} + \frac{\partial^2 p}{\partial y^2} + \frac{\partial^2 p}{\partial z^2} \right), \tag{1}$$

where $p = p(x, y, z, t)$ is the acoustic pressure and c the speed of sound, taken here to be 344 m/s. Equation (1) can be discretized by substituting the partial derivatives with finite differences. The numerical scheme used in this work is referred to as *standard rectilinear* (Kowalczyk and van Walstijn, 2011), where the boundary conditions are implemented as first-order accurate approximations (Webb and Bilbao, 2011). The update equation for the entire domain reads

$$p_{k,l,m}^{n+1} = \frac{1}{1 + \lambda \beta} \left[(2 - K\lambda^2)p_{k,l,m}^n + (\lambda \beta - 1)p_{k,l,m}^{n-1} + \lambda^2 (p_{k+1,l,m}^n + p_{k-1,l,m}^n + p_{k,l-1,m}^n + p_{k,l+1,m}^n + p_{k,l,m-1}^n + p_{k,l,m+1}^n) \right], \tag{2}$$

where $\beta = (6 - K)/2\xi$ and ξ is the specific acoustic impedance of the boundary node. The variable K indicates the

number of neighboring air cells present in the node, and $\lambda = c\Delta t/\Delta x$ denotes the Courant number, where Δx is the spatial step size and Δt the sampling interval. In this study, the Courant number is limited for stable free-field time stepping (i.e., $\lambda = 1/\sqrt{3}$).

III. ANALYSIS

The analysis of the SDE regarding the geometrical properties of the seating area and the individual seats is carried out in three parts covering different purposes.

A preliminary analysis regarding the resolution of the simulation is conducted in order to assess the numerical error associated with the FDTD method. In this preliminary analysis constituting the first part of the analysis, the accuracy of the simulated results is evaluated by a grid refinement study. In the second part of the analysis, FDTD simulations of three parameterized hall models are run for a wide range of seat parameter values. The frequency range considered in the first two parts of the analysis is 20–1000 Hz. The third part of the analysis consists in analyzing the temporal evolution of the frequency components in the parameterized hall models for the seat parameter values that are found relevant in the second part of the analysis.

A. Determination of the simulation accuracy

A preliminary analysis is carried out to examine the deviation of the FDTD solution acquired with a fixed sampling frequency in comparison to an asymptotic prediction. The asymptotic prediction is computed using a series of FDTD simulations run with different grid spacings and a linear regression model for the convergence, following a similar procedure to that of Meyer *et al.* (2023), Meyer *et al.* (2022), and Prepeľiță *et al.* (2019). The lowest possible convergence rate is assumed, that is the first-order accuracy of the boundary model, and the following regression model based on the magnitude spectrum of the simulation results reads

$$|\hat{F}_{i,s,r}(\omega, \Delta X_i)| = |F_{s,r}(\omega)| + C(\omega)\Delta X_i, \quad (3)$$

where \hat{F}_i is the i th FDTD solution acquired with a spatial discretization step of ΔX_i representing the transfer function between the source s and receiver r . F is the sought asymptotic prediction and $C(\omega)$ denotes the coefficient of the principal error term.

An open-source FDTD solver (Saarelma and Savioja, 2014) implementing Eq. (2) was utilized to run the simulations. A total of 10 simulations were run with different grid spacing related to each other by a grid refinement ratio of $\tau = 1.1$ [minimum recommended in practice (Roache, 1998, p. 124)]. A *soft* source with a low-pass filtered (using a finite impulse response filter of 128 samples with a cutoff frequency set to 2 kHz and a Hanning window) Kronecker delta as the source excitation signal was employed for all the simulations. In addition to the low-pass filter, a DC-block filter with a cutoff frequency of 5 Hz was applied to

the source signal. This preliminary analysis was conducted on the *shoebox* hall condition with a *stage height* of 0.5 m and with *step* conditions 0.0 and 0.2 m as well as with *underpass* conditions 0.0 and 0.4 m (see also Table I and Figs. 1 and 3), resulting in a total of four parameter conditions. A single source-receiver combination was considered to compute the asymptotic predictions. The source position corresponded to one of the source position conditions investigated in the second part of the analysis (Sec. III B) which locates at a height of 1 m from the stage floor and is the closest to the surrounding side walls. The receiver position was also chosen based on the receiver position conditions from the second part of the analysis such that it was located in the middle of the seating area of the *shoebox* hall condition (at the 13th row). In a post-processing stage, the FDTD solutions were time-windowed from the arrival of the direct sound using a 20 ms rectangular window, and their magnitude spectrum was one-third octave band smoothed. The source-receiver distance was also compensated for each individual response.

The 95% confidence intervals (CIs) on the asymptotic predictions were obtained using the bias-corrected and accelerated bootstrap method (with 1000 samples) (Efron, 1987). The results of the preliminary analysis, shown in Figs. 2(a)–2(d), demonstrate that the asymptotic predictions are close to the FDTD solutions using $\Delta X = 0.02$ m. To quantify the deviation of the FDTD solutions with respect to the asymptotic predictions, hit rates were computed as the number of frequency bins (in %) for which each FDTD solution is within the 95% CIs of the asymptotic predictions. The hit rate was the largest using $\Delta X = 0.02$ m for one of the four parameter conditions and within the fourth largest for the three remaining conditions. These results indicate that the deviation of the FDTD solutions ran with $\Delta X = 0.02$ m compared to the asymptotic predictions is relatively small. As such, the smallest ΔX is considered satisfactory to run the FDTD simulations in the present context and will be employed in the following.

B. Simulations of the SDE with varying parameters

A series of FDTD simulations of three parameterized hall models are executed in this second part of the analysis. The independent variables are *step*, *underpass*, *stage height*, *source position*, and *hall* and the dependent variables are the impulse responses between each source and respective

TABLE I. The levels of each independent variable used in the second part of the analysis.

Independent variable	Levels
Step	{0.0 m, 0.2 m, 0.4 m, 0.6 m}
Underpass	{0.0 m, 0.2 m, 0.4 m}
Stage height	{0.5 m, 1.0 m, 1.5 m}
Source position ^a	{0, 1, 2, 3, 4, 5}
Hall	{shoebox, surround, fan}

^aRefer to Fig. 1 to visualize the positions in each hall.

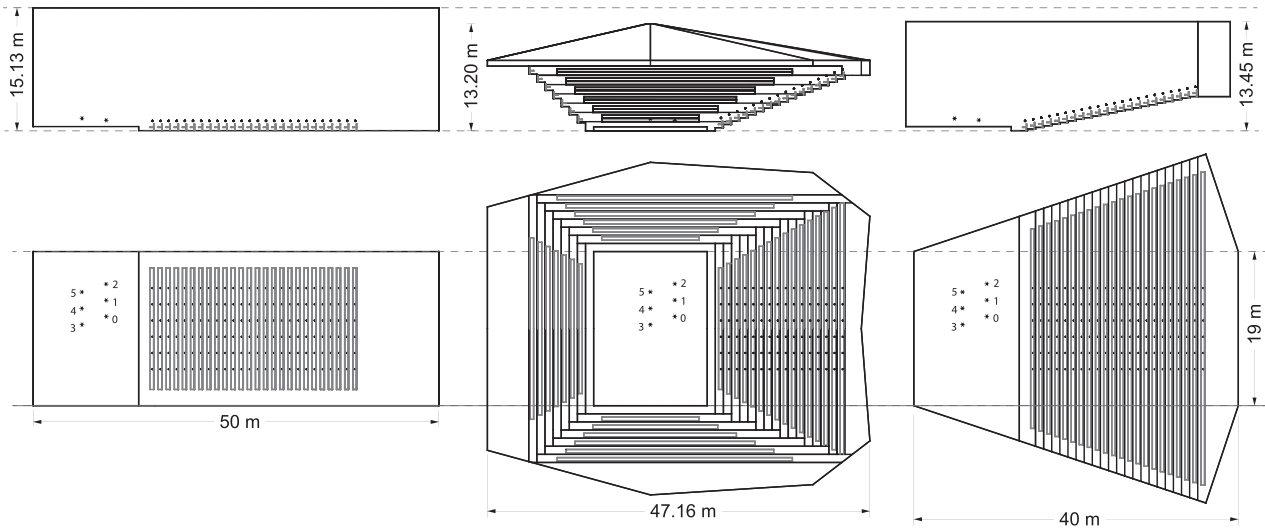


FIG. 1. Cross-section (top) and floor plan (bottom) of the shoebox (left), surround (middle), and fan (right) hall model. Source locations are indicated as asterisk symbols and receiver locations as circles. The height of each hall type is adjusted so that the volume is fixed to 14 250 m³ for the three hall conditions.

receiver positions for each of the independent variable levels. The independent variables *step* and *underpass* are illustrated in Fig. 3 while the levels of each independent variable are listed in Table I.

Three different hall geometries, which resemble the typical shapes of a shoebox, a vineyard, and a fan hall geometries are considered, although here the condition resembling a vineyard hall is referred to as *surround* due to

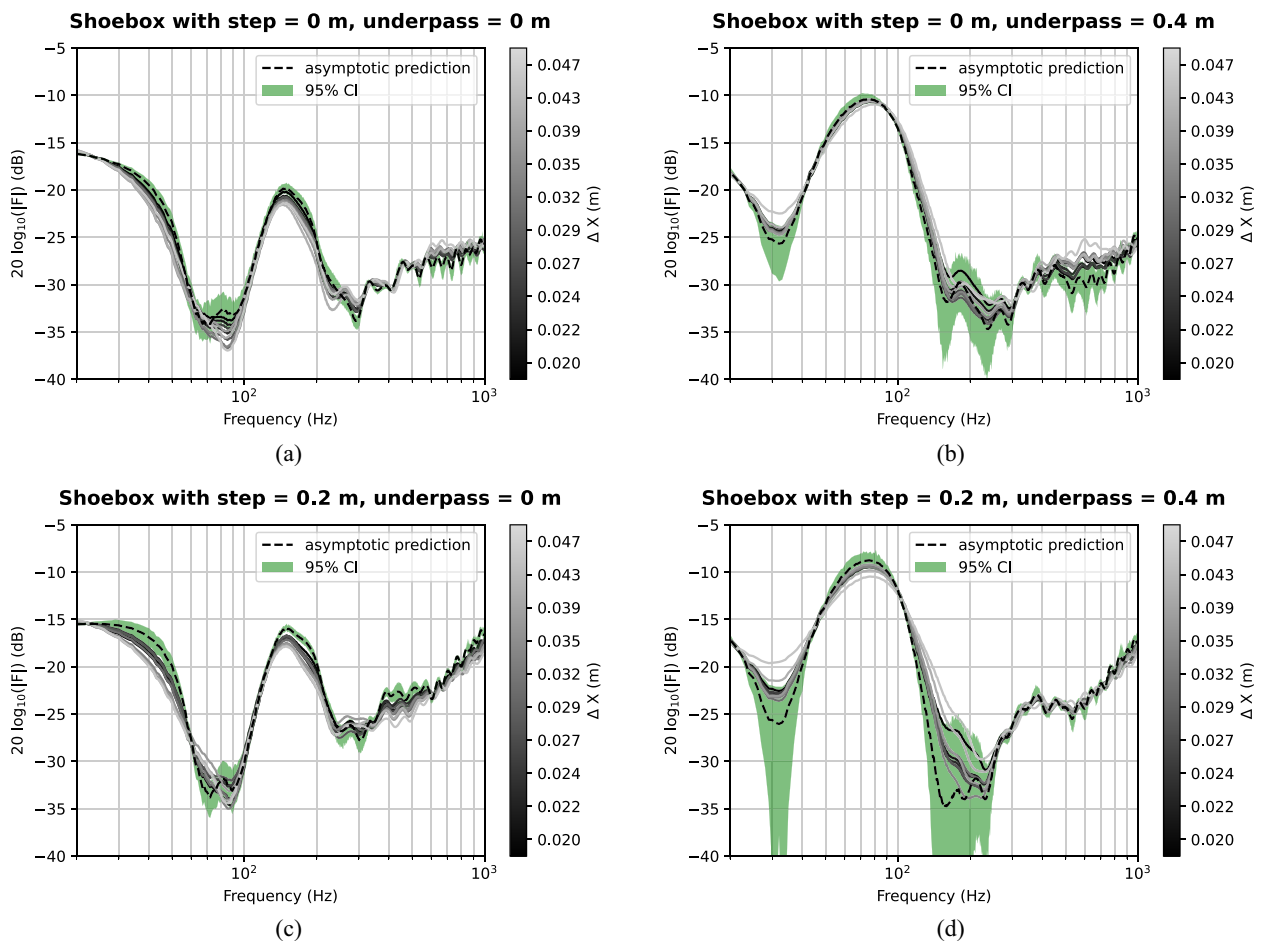


FIG. 2. (Color online) Magnitude spectrum of the individual FDTD solutions with respective spatial grid spacings ΔX , asymptotic prediction computed from the first-order asymptotic model from Eq. (3), and the 95% CI for the shoebox hall with (a) *step* 0.0 m and *underpass* 0.0 m, (b) *step* 0.0 m and *underpass* 0.4 m, (c) *step* 0.2 m and *underpass* 0.0 m, and (d) *step* 0.2 m and *underpass* 0.4 m.

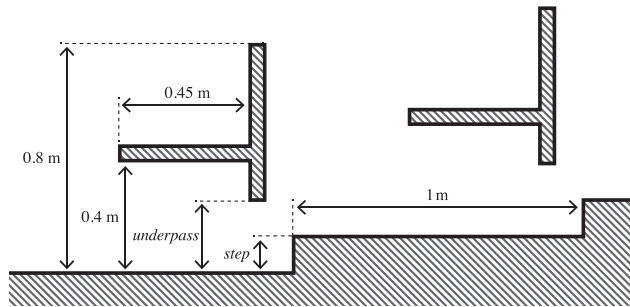


FIG. 3. Illustration of the different parameters of the seating geometry.

obvious discrepancies in the seating layout. The volume of the three hall conditions is fixed to $14\,250\text{ m}^3$, which is the volume of the empty shoebox model without the seating. The hall volume is normalized for each *step* condition by adjusting the ceiling height. The volume values of each hall condition may be considered representative for the respective hall type, though, for the *surround* and *fan* hall conditions, it can be considered to be slightly underestimated in comparison to real halls of these types. However, here the equal volume with the *shoebox* hall condition is of interest regarding the comparisons.

In addition, it is acknowledged that the three hall conditions are fairly crude simplifications of the geometries of real counterparts of the respective hall type. As such, the models hardly contain any scattering surface details except the seating area, and none of the hall models has balconies, stalls, or ceiling reflectors, which are present in most existing halls. The simplified hall models aim to reproduce some very general phenomena typical to the overall shape of each hall in such a way that the results are comparable. Here, the typical traits of each hall are considered to be parallel side walls, a large length of the hall, a high ceiling (*shoebox*), sidewalls in an angle with a widening seating area (*fan*), and a seating area surrounding the stage area so that early energy is mostly arriving from reflections from the ceiling and the seating area (*surround*). From these three hall conditions, the condition *surround* may be considered to deviate the most from real vineyard-style halls conceptually. Therefore, the results relating to this hall condition should be interpreted with additional caution.

The source and receiver positions used in the simulations are illustrated in Fig. 1. The six source positions are located on the stage in two rows so that all the positions are on one side of the stage. The source row closest to the edge of the stage is at a height of 0.8 m, whereas the second source row is at a height of 1.0 m from the stage floor. The receiver positions are placed at the height of 1.2 m from the floor at each seat row.

The analysis can be considered to be a full factorial type [Montgomery (2001, p. 170)] with a few exceptions. For the *surround* hall condition, only *step* conditions 0.2, 0.4, and 0.6 m are simulated, as halls of this type with a flat floor generally do not exist. In addition, the number of seat rows in the main audience differs for each hall type.

The number of seat rows for the hall conditions *shoebox*, *surround*, and *fan* are 26, 16, and 22, respectively.

Unless otherwise stated, the illustrations use the following convention: each level of an independent variable is represented with a different color, the mean value of each frequency bin within that level is represented with a thick continuous line, and the translucent region that is framed by the dashed lines indicates the region in which 95% of the data falls into. The responses that are time-windowed with a 20 ms window are distance compensated according to the source-receiver distance of each pair so that the characteristics of the SDE on the direct sound can be studied. The responses which are windowed with a 500 ms window are not distance compensated.

1. Step/inclination

It has been suggested that the SDE ameliorates upon increasing inclination (Schultz and Watters, 1964). When the simulation data is analyzed for different step sizes in Fig. 4(a), two dips can be seen. The dip at around 250 Hz becomes shallower with increasing inclination, thus relating to the previous observations on the SDE. The other dip at 100 Hz exists for some step sizes only, and its existence can be explained by the absence or blocking of the seat underpasses. Namely, the dip at 100 Hz occurs for the step sizes of 0.4 and 0.6 m that always block the underpass (max. 0.4 m). In turn, for smaller step sizes where the underpass may or may not be blocked, this lower dip is not clearly visible in the average response. Yet, the dip can be observed in the variability in 95% interval of the magnitude spectrum, as there are also closed seats (*underpass* 0 m) on the flat floor (*inclination* 0 m), and closed and small *underpass* (0.2 m) on the smallest *step size* (0.2 m).

Apart from the dips, the level below 100 Hz and above 200 Hz increases with inclination. The level increase above 200 Hz can be explained by increased positive diffraction from the tops of the seat backrest in front of the receiver (Tahvanainen et al., 2020). At 500 ms after the direct sound, these differences have almost disappeared as shown by Fig. 5(a). Thus, the step size or inclination does not seem to have a large influence on the late response of the concert hall.

2. Underpass

The results grouped by underpass size in Fig. 4(b) show that the first dip at about 100 Hz is heavily influenced by the underpass size while the second dip at 250 Hz stays more constant. In addition, the low-frequency energy increases with increasing underpass size. When the effect of the step size on the blocking is taken into account, Fig. 4(c) shows clearly that the underpass must be free from blockage to increase the low-frequency level between 40 and 100 Hz. This corroborates the speculations by Davies (1992) and the observations in scale model measurements by Tahvanainen et al. (2020).

At 500 ms after the direct sound, the absence or the blockage of the underpass still seems to carry the dip at 100 Hz, as shown by Figs. 5(b) and 5(c). In other words,

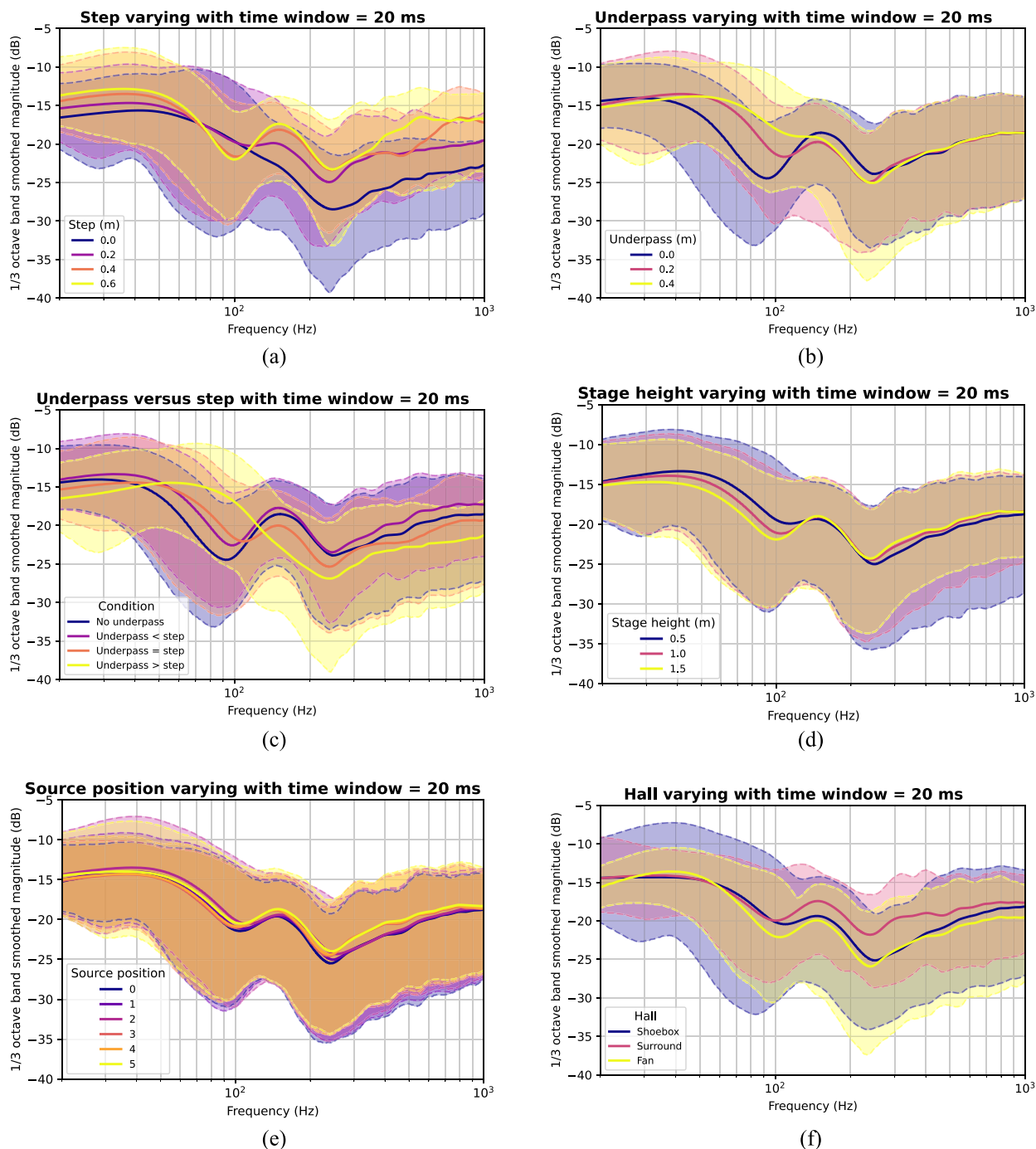


FIG. 4. (Color online) One-third octave band smoothed magnitude spectrum at different levels of the condition (a) *step*, (b) *underpass*, (c) of groups where there is no *underpass* (i.e., where the seat is closed), the *underpass* is smaller or equal than the *step*, the *underpass* is equal than the *step*, or the *underpass* is greater than the *step*, (d) *stage height*, (e) *source position*, and (f) *hall*, averaged over all the other conditions. A rectangular time window of 20 ms from the arrival of the direct sound at each receiver position is utilized. Distance compensation is used for each individual response.

open seats can increase the level by 3–5 dB at around 100 Hz at 500 ms after the direct sound.

3. Stage height

The results grouped by stage height in Fig. 4(d) indicate that a smaller stage height leads to a larger variability in 95% interval of the magnitude spectrum at higher frequencies. More precisely, it can be seen that for the *stage height*

condition 0.5 m, the 95% interval of the data exhibits a magnitude spectrum approximately 5 dB lower than for the 1.5 m *stage height* condition between 300 Hz and 1 kHz. Also, the second dip at about 250 Hz is deeper with a smaller stage height. These observations are similar to the measurement results if the angle of arrival of the direct sound is considered: the lower the stage, the closer the arrival angle to the plane formed parallel to the tops of the seat backrests

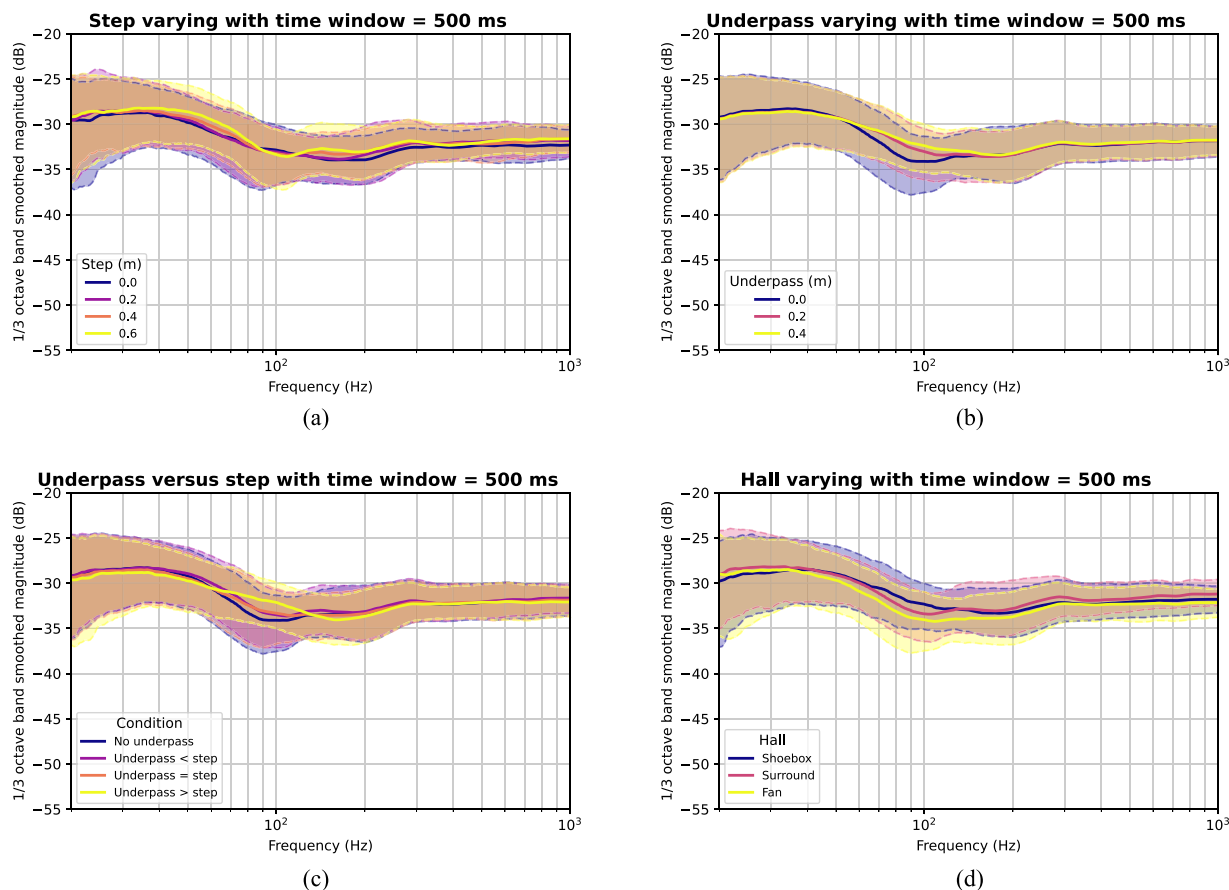


FIG. 5. (Color online) One-third octave band smoothed magnitude spectrum at different levels of the condition (a) *step*, (b) *underpass*, (c) of groups where there is no *underpass* (i.e., where the seat is closed), the *underpass* is smaller or equal than the *step*, the *underpass* is equal than the *step*, or the *underpass* is greater than the *step*, and (d) *hall*, averaged over all the other conditions. A rectangular time window of 500 ms from the arrival of the direct sound at each receiver position is utilized. No distance compensation is used.

(Davies, 1992; Ishida, 1993; Schultz and Watters, 1964; Sessler and West, 1964). Interestingly, the first dip at about 100 Hz ameliorates with decreasing stage height. Furthermore, the magnitude spectrum below 100 Hz for the lowest stage height (i.e., *stage height* of 0.5 m) is a few dB higher than for the other stage height conditions for the given 20 ms analysis time window.

The influence of the stage height was however almost non-visible on the magnitude spectrum when a 500 ms time window was applied to the simulated impulse responses (results not shown).

4. Source position

As shown in Fig. 4(e), the source position has little influence across the frequency response in comparison to the other independent variables considered. Though the influence of the source position is subtle, it can be seen from Fig. 4(e) that the effect at higher frequencies is similar to what was observed for the stage height. More specifically, the variability at higher frequencies is larger for the *source position* conditions 0, 1, and 2 compared to *source position* conditions 3, 4, and 5. This result is in line with the relationship between the source position and the stage height variables.

In fact, *source position* 5 gives the larger angle of incidence while *source position* 0 gives the most grazing angle of incidence, thus relating to a higher and smaller stage height, respectively.

The influence of the source position was even smaller than shown in Fig. 4(e) when a 500 ms time window was applied to the simulated impulse responses (results not shown).

5. Hall

The results grouped by hall type are shown in Figs. 4(f) and 5(f) for two different time windows. As can be seen in Fig. 4(f) the variability in 95% interval of the magnitude spectrum is larger in the shoebox hall than in the other halls, in particular below 100 Hz. However, the differences become smaller with time, and a dip at 100 Hz is the least pronounced in the shoebox hall [Fig. 5(f)].

To better understand the effect of the interaction between the *step* and *underpass* conditions in each hall, Fig. 4(c) has been reproduced for each hall separately in Fig. 6. It can be seen that the variability in 95% interval of the magnitude spectrum at 20 ms is the smallest in the surround hall, probably due to early reflections from the surrounding seats, and due to the fact that the cases involving the flat

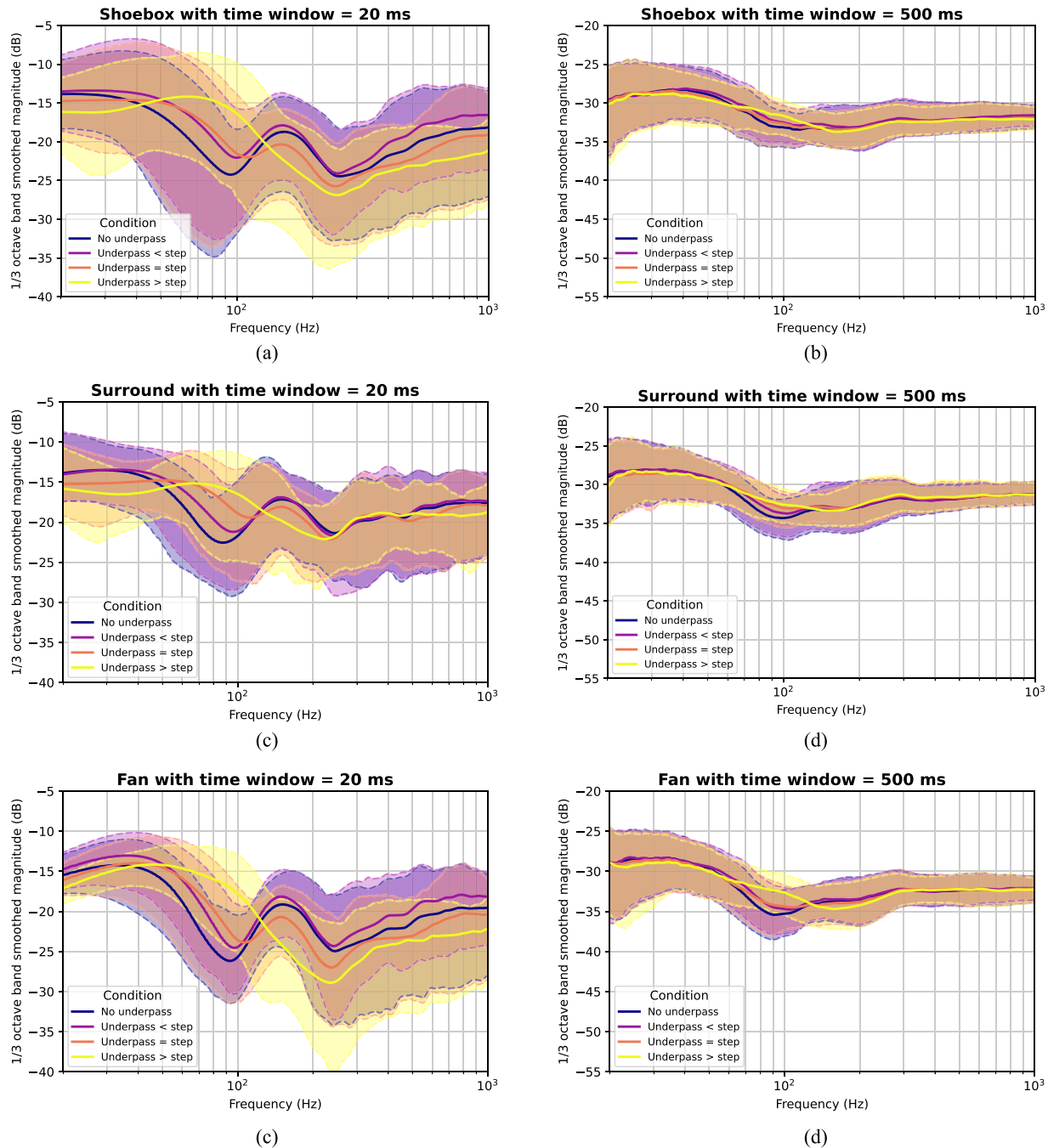


FIG. 6. (Color online) One-third octave band smoothed magnitude spectrum of groups where there is no *underpass* (i.e., where the seat is closed), the *underpass* is smaller or equal than the *step*, the *underpass* is equal than the *step*, or the *underpass* is greater than the *step* for the (a), (b) shoebox hall, (c), (d) surround hall, (e), (f) fan hall, with a rectangular time window of (left column) 20 ms and (right column) 500 ms from the arrival of the direct sound at each receiver position is utilized, respectively.

floor and thus more cases of open seats were not simulated. Especially, the dip at 250 Hz seems to benefit from such reflections. With a seated audience, such reflections are likely to diminish. The largest variability in 95% interval of in the magnitude spectrum occurs in the shoebox hall and similar observations have been made with the measurements (Tahvanainen *et al.*, 2015a). Finally, it should be noted that the level between 80 and 100 Hz always is highest when the underpass is larger than the step size regardless of the hall type or the analysis time window.

C. Visualization of cumulative energy in the frequency domain

In this third part of the analysis, several parameter values that were found relevant to the SDE in Sec. III B are chosen to explore the effects in the frequency domain caused by the different geometries. The frequencies of interest are selected based on the dips that were observed in the previous part. The method described in Saarelma and Savioja (2019) is used to produce animations showing the

spatial analysis of the time-frequency evolution in the chosen halls. The animations (some snapshots are shown in Fig. 7) visualize the typical propagation of sound waves in time, but also the cumulative energy at each point in the x-y and x-z cross-sections of the halls and at selected frequencies, revealing areas that suffer the lack of cumulative energy over the entire analysis time window. As a reminder, the full videos for several cases and frequencies are included as supplementary material.¹ All the animations, which were generated from FDTD simulations using a spatial grid spacing of 0.02 m, are for the halls with the *source position* condition 0 and *stage height* condition 0.5 m.

Figure 7 shows two snapshots of visualization of the spatial time-frequency evolution in a shoebox-shaped hall [i.e., cases in Fig. 6(a)]. Figure 7(a) shows an example of closed seats at 100 Hz while the entire animation for this condition is provided in SuppPubmm4.mov. At 48 ms, a darker area (corresponding to the first dip at around 100 Hz) spans across all seats at ear level. Similar observations can be made for closed seats in other floor inclinations and concert hall shapes (see, e.g., the supplementary material SuppPubmm1.mov). For the shoebox hall with open seats shown in Fig. 7(b) and in the supplementary material SuppPubmm5.mov, the same area is bright, indicating a boost of cumulative energy at this particular frequency. A similar behavior is also observed for other halls with open

or partially open seats and different floor inclinations (see, e.g., supplemental materials SuppPubmm2.mov and SuppPubmm3.mov). Figures 7(c) and 7(d) show the corresponding setting but at the center frequency of 250 Hz, corresponding to the second dip observed in most conditions. The darker area spans several seat rows at once and worsens across the seat rows traveled. As time advances, the ceiling and floor reflections clearly mitigate the dip (the darker areas reduce in the front seats), but there is an interplay between the seat geometry and the concert hall shape. Namely, in the shoebox hall with open seats (i.e., with a 0.4 m *underpass*), the SDE has recovered already with the first side reflection at the first seats, as can be seen in Fig. 7(d) and in the animation SuppPubmm13.mov provided as supplementary material. However, in the shoebox hall with closed seats shown in Fig. 7(c) and in the animations SuppPubmm12.mov and SuppPubmm14.mov provided as supplementary material, the first side reflection does not fill in the energy yet, and a ceiling reflection is needed. Further analysis of the videos (see, e.g., the supplementary videos SuppPubmm9.mov, SuppPubmm10.mov, SuppPubmm11.mov, and SuppPubmm15.mov) reveals that in the fan-shaped hall, the first ceiling reflection fills in the SDE, for both open and closed seats, but the recovery takes a longer time, as there are no side reflections. This result is similar to the experimental observations that the SDE recovers fastest in concert

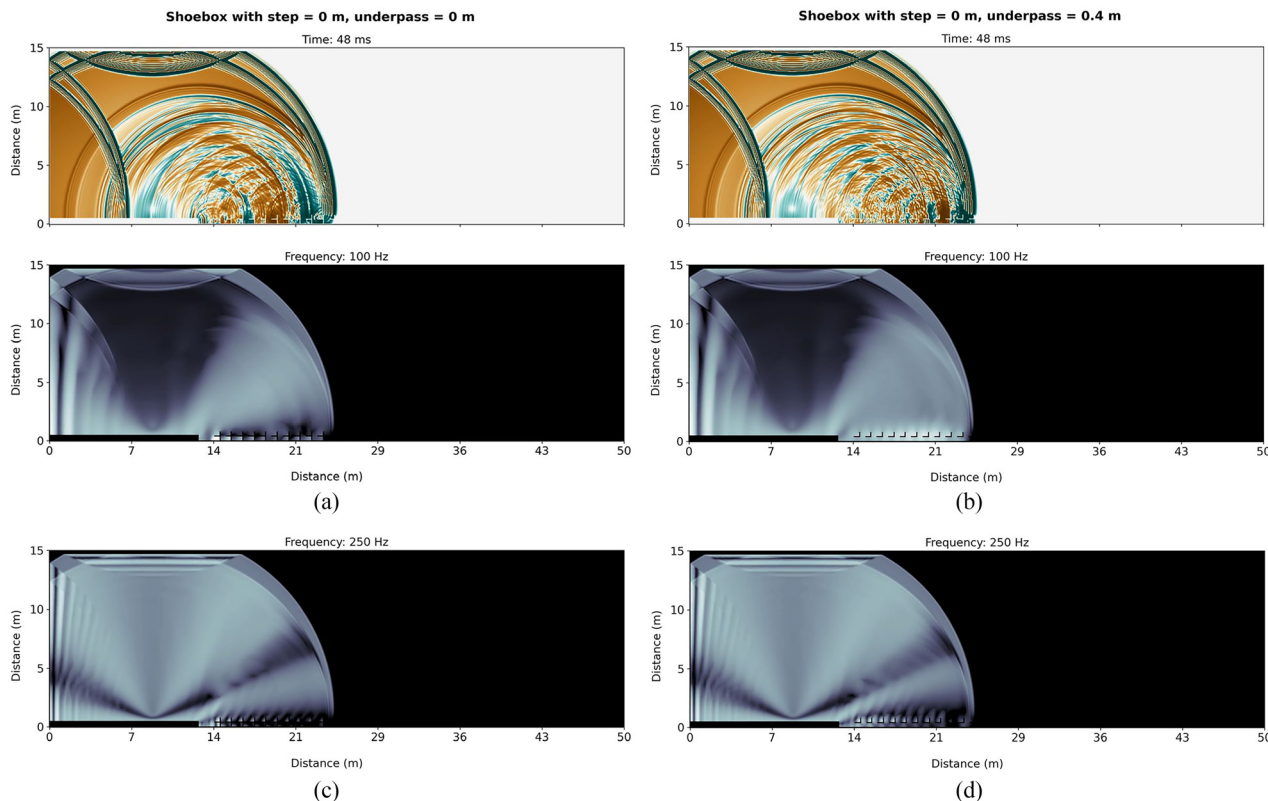


FIG. 7. (Color online) Snapshot of the animations showing the spatial distribution of the time-domain pressure field (top) and the cumulative frequency domain energy (bottom) in the *shoebox* hall at time 48 ms and at the center frequency 100 Hz for the condition (a) *underpass* 0.0 m and (b) *underpass* 0.4 m. (c) and (d) correspond to the same conditions as in (a) and (b) but for the center frequency 250 Hz. The color range in each cumulative frequency domain energy visualization is [-25, 0] dB, while that of the time-domain wavefront is [-40, 40] dB.

halls with enveloping late energy (Tahvanainen *et al.*, 2015a). Finally, the attenuation at both frequency bands worsens with distance, as has been observed with measurements (Bradley, 1991; Davies, 1992; Ishida, 1993; Schultz and Watters, 1964; Sessler and West, 1964; Tahvanainen *et al.*, 2015a).

The remainder of the videos provided as supplementary materials as SuppPubmm6.mov, SuppPubmm7.mov, and SuppPubmm8.mov show how the energy accumulates at 150 Hz, which appears as a peak between the two dips in the responses of the previous part. At this frequency, there is a positive interference from the horizontal seat bottoms. For the closed seats, short-term attenuation is also created at ear height for the first 5 ms after the arrival of the direct sound, while for the open seats, this attenuation is higher above the seats.

IV. DISCUSSION

The simulations corroborate many of the experimental observations on the SDE and provide some additional details, especially by visualizing the phenomena. Regarding the results of the parametric study, in many conditions a double-dip of the SDE can be observed. The first dip occurs between 80 and 100 Hz when there is no underpass or when the underpass is blocked (step size is larger than underpass). The attenuation ameliorates with decreasing stage height. The $1/4$ wavelength at this center frequency corresponds approximately to the effective seat backrest height, as measured from the seat top to the step behind the seat. For the blocked seats, this dip is not as severe as for the closed seats.

A second dip occurs at around 250 Hz in all cases, and initially it is the deepest dip when the underpass is larger than the step size (i.e., for open seats) while its frequency does not seem to change that much. In addition, this second dip ameliorates with increasing step size/inclination and worsens with increasing stage height. The second dip is recovered with late reverberation as seen in Fig. 5, while the first dip tends to somewhat remain even with late reverberation. The $1/4$ wavelength at this center frequency corresponds approximately to the height of the seat bottom.

Interestingly, such a double-dip behavior is rarely observed in the measurements. Bradley (1991) attributed the double-dip behavior to both horizontal and vertical resonances between the seats. Here, the double dip could be related to the seat bottom being horizontal, as the second dip is present in all cases. While in most measured concert halls the seat bottom is actually tipped up and only a single dip is observed, a double dip was observed in the scale model measurements with horizontal seat bottoms (Tahvanainen *et al.*, 2020). Furthermore, such a double dip has been observed in measurements with a seated audience (Tahvanainen and Lokki, 2018).

The visualisations of simulations reveal more about the nature of the double dip. Namely, the two dips have very different attenuation patterns, as illustrated in Fig. 7 with both open and closed seats in the shoebox hall with a flat floor. The patterns have similar differences on inclined floors in other halls,

as well. For the first dip at 100 Hz, the attenuated layer can be observed over the closed seats but with open seats no attenuation is seen. When analyzing the supplementary videos, it can be seen that the seats act as a secondary source. With open seats, this secondary wavefront can propagate across the seating area despite the seat backrest, creating a positive interference just above the seat rows at ear height. For closed seats, the secondary wavefront is restricted by the seat backrest that extends to the floor, thus enforcing an attenuation to form at ear height and to travel across successive seat rows. In addition, side and ceiling reflections create new attenuation patterns at ear height while reducing the original attenuation. This could explain why the first dip persists in all halls with closed seats after 500 ms (see Fig. 6). As the attenuation persists regardless of the direction of the arriving reflections, it could be related to the vertical resonance phenomenon mentioned by Bradley (1991), Min and Liao (2021), and Sessler and West (1964).

For the second dip at 250 Hz, the attenuation spans over several seat rows with a diagonal pattern and it is present from the second row onwards. There appears to be a secondary source both under and on top of the horizontal seat bottom, and the sound is reflected off the top of the seat bottom. As time progresses, these secondary sources create a standing wave pattern between the top parts of the consecutive seats and thus an attenuation front that covers the entire seat above ear height. For closed or blocked seats, the attenuation pattern remains on all seat rows until the first reflections arrive, while for the open seats, the attenuation propagates. When inclination increases, a clear standing wave pattern no longer forms between the top parts of consecutive seats, and consequently, the attenuation at ear height is lessened. The attenuation is lessened by the reflections from the hall, but traces of it remain visible even at 200 ms in the supplementary videos.

As for the other studied parameters, increasing the inclination of the seating area increases the sound energy above 200 Hz. Naturally, the possible audience absorption and directivity of the musical instruments will also have an influence in this frequency range in real life conditions. An increase in the stage height, which in fact increases the angle of incidence and relates to the source position, shows a minor effect on the SDE. The change in the angle of incidence due to the change in stage height corresponds to about 9° at 10 m, which is a considerably smaller change than what was studied in previous research with single source-receiver pairs (Sessler and West, 1964; Takahashi, 1997). The source position is found to have little influence on the SDE, although, in some experiments investigating a single case, some variations can be detected.

Finally, while the present results do not involve perceptual aspects of the SDE, some of the implications of results can be discussed. Previously, it was found that when audible, the listeners prefer a direct sound that is not affected by the SDE (Tahvanainen *et al.*, 2017). However, in that study, the frequencies below 100 Hz were not modified, and therefore the results might have been different with a more realistic consideration of the sound level below 100 Hz. The

current study shows that the seats with underpass provide always stronger sound than the closed seats between 60 and 120 Hz, which is an important frequency range for low-register instruments in the symphony orchestra. These low-register instruments were perceived to have a higher level of bass and sometimes also higher clarity in shoebox halls with seats with underpasses than in vineyard-shaped halls with closed seats (Tahvanainen *et al.*, 2015b). Consequently, having underpasses might be beneficial for the perception of the acoustics in performance spaces.

V. CONCLUSIONS

Using FDTD simulations, the SDE was investigated in three parameterized halls of representative shapes and in terms of several geometric properties of the seating area, namely, the underpass size, step size, stage height, and source position. The aim was to identify the relative contribution of each of these parameters to the SDE with a larger set of responses than what could be obtained with measurements alone.

The results show that the two major parameters affecting the SDE are the size of the underpass (the space between the floor and the seat backrest) and the step size of the raking floor defining the overall inclination of the seating area. The results show the significance of the underpass on the low-frequency response below 100 Hz and the floor inclination of the high-frequency response between 200 and 1000 Hz. On the contrary, the stage height and source position have a very small overall effect on the SDE.

The SDE is also confirmed to be mostly occurring in the early part of the room response as demonstrated by the comparisons of the 20 and 500 ms time-windowed responses transformed to the frequency domain. In addition, the results suggest that two attenuation dips form at different frequencies and they recover differently. At around 100 Hz, the initial attenuation at 20 ms, typical to closed seats, spans a smaller area but is regenerated with reflections. At 250 Hz, the initial attenuation, often the strongest with seats with an underpass, spans a larger area and is mitigated by the reflections. Here, with the ceiling reflections, the recovery happens later than with some early side reflections.

Finally, this paper provides (as supplementary material¹) several animations showing the spatial-time evolution of the sound field at specific frequencies in some of the halls and seating configurations investigated. These animations visually demonstrate the effect of the most important geometric seat features responsible for the SDE.

¹See supplementary material at <https://doi.org/10.1121/10.0020826> for animations showing the spatial time-frequency evolution in several halls.

Ando, Y., Takaishi, M., and Tada, K. (1982). "Calculations of the sound transmission over theater seats and methods for its improvement in the low-frequency range," *J. Acoust. Soc. Am.* **72**(2), 443–448.
 Bradley, J. S. (1991). "Some further investigations of the seat dip effect," *J. Acoust. Soc. Am.* **90**(1), 324–333.
 Davies, W. (1992). "The effects of seating on the acoustics of auditoria," Ph.D. thesis, University of Salford, Salford, UK.

Davies, W., and Cox, T. (2000). "Reducing seat dip attenuation," *J. Acoust. Soc. Am.* **108**(5), 2211–2218.
 Efron, B. (1987). "Better bootstrap confidence intervals," *J. Am. Stat. Assoc.* **82**(397), 171–185.
 Fratoni, G., Hamilton, B., and D’Orazio, D. (2022). "Feasibility of a finite-difference time-domain model in large-scale acoustic simulations," *J. Acoust. Soc. Am.* **152**(1), 330–341.
 Ishida, K. (1993). "The measurement and prediction of sound transmission over auditorium seats," Ph.D. thesis, University of Cambridge, Cambridge, UK.
 Ishida, K. (1995). "Investigation of the fundamental mechanism of the seat-dip effect using measurements on a parallel barrier scale-model," *J. Acoust. Soc. Jpn. (E)* **16**(2), 105–114.
 Kawai, Y., and Terai, T. (1991). "Calculation of sound fields over audience seats by using integral equation method," *J. Vib. Acoust.* **113**(1), 22–27.
 Kowalczyk, K., and van Walstijn, M. (2011). "Room acoustics simulation using 3-D compact explicit FDTD schemes," *IEEE Trans. Audio. Speech. Lang. Process.* **19**(1), 34–46.
 Lokki, T., Southern, A., and Savioja, L. (2011). "Studies on seat dip effect with 3D FDTD modeling," in *Proceedings of Forum Acusticum*, Aalborg, Denmark, pp. 1553–1558.
 Lokki, T., Southern, A., Siltanen, S., and Savioja, L. (2013). "Acoustics of epidaurus—Studies with room acoustics modelling methods," *Acta Acust. united Acust.* **99**(1), 40–47.
 LoVetri, J., Mardare, D., and Souldre, G. (1996). "Modeling of the seat dip effect using the finite-difference time-domain method," *J. Acoust. Soc. Am.* **100**(4), 2204–2212.
 Meyer, J., Prepeljč, S., Khajeh-Saeed, A., Smirnov, M., and Hoffmann, P. (2023). "Verification on head-related transfer functions of a snowman model simulated using the finite-difference time-domain method," *IEEE/ACM Trans. Audio. Speech. Lang. Process.* **31**, 2579–2591.
 Meyer, J., Smirnov, M., Khajeh-Saeed, A., Hoffmann, P. F., and Prepeljč, S. T. (2022). "Finite-difference time-domain simulations: Verification on head-related transfer functions of a rigid sphere model," *JASA Express Lett.* **2**(6), 062401.
 Min, H., and Liao, Y. (2021). "Mechanism analysis of the influence of seat attributes on the seat dip effect in music halls," *Appl. Sci.* **11**(20), 9768.
 Mommertz, E. (1993). "Attenuation of sound passing over audience at grazing incidence," *J. Acoust. Soc. Am.* **93**(4), 2303.
 Montgomery, D. C. (2001). *Design and Analysis of Experiments*, 5th ed. (Wiley, New York).
 Oberkampf, W. L., and Roy, C. J. (2010). *Verification and Validation in Scientific Computing* (Cambridge University Press, Cambridge, UK).
 Osa, T., Murakami, K., Horinouchi, Y., and Takahashi, D. (2007). "Application of audience-seats characteristics to the sound field analysis for large enclosures," *Appl. Acoust.* **68**, 939–952.
 Pätynen, J., Tervo, S., and Lokki, T. (2013). "Analysis of concert hall acoustics via visualizations of time-frequency and spatiotemporal responses," *J. Acoust. Soc. Am.* **133**(2), 842–857.
 Prepeljč, S. T., Gómez Bolaños, J., Geronazzo, M., Mehra, R., and Savioja, L. (2019). "Pinna-related transfer functions and lossless wave equation using finite-difference methods: Verification and asymptotic solution," *J. Acoust. Soc. Am.* **146**(5), 3629–3645.
 Roache, P. J. (1998). *Verification and Validation in Computational Science and Engineering* (Hermosa, Albuquerque, NM), Vol. 895.
 Saarelma, J., and Savioja, L. (2014). "An open source finite-difference time-domain solver for room acoustics using graphics processing units," in *Proceedings of Forum Acusticum*, Krakow, Poland, p. SS11.8.
 Saarelma, J., and Savioja, L. (2019). "Spatial analysis of modal time evolution in room acoustics," *J. Acoust. Soc. Am.* **145**(1), EL116–EL121.
 Sakurai, Y., Morimoto, H., and Ishida, K. (1993). "The reflection of sound at grazing angles by auditorium seats," *Appl. Acoust.* **39**(3), 209–227.
 Schultz, T. J., and Watters, B. (1964). "Propagation of sound across audience seating," *J. Acoust. Soc. Am.* **36**(5), 885–896.
 Sessler, G., and West, J. (1964). "Sound transmission over theatre seats," *J. Acoust. Soc. Am.* **36**(9), 1725–1732.
 Tahvanainen, H. (2021). "Analysis and perception of the seat-dip effect in concert halls," Ph.D. thesis, Aalto University, Espoo, Finland.
 Tahvanainen, H., Haapaniemi, A., and Lokki, T. (2017). "Perceptual significance of seat-dip effect related direct sound coloration in concert halls," *J. Acoust. Soc. Am.* **141**(3), 1560–1570.

- Tahvanainen, H., and Lokki, T. (2018). "About the seat-dip effect in the presence of audience," in *Proceedings of the International Congress of Sound and Vibration*, Hiroshima, Japan.
- Tahvanainen, H., Lokki, T., Jang, H.-S., and Jeon, J.-Y. (2020). "Investigating the influence of seating area design and enclosure on the seat-dip effect using scale model measurements," *Acta Acust.* **4**(4), 15.
- Tahvanainen, H., Pätynen, J., and Lokki, T. (2015a). "Analysis of the seat-dip effect in twelve european concert halls," *Acta Acust. united Acust.* **101**(4), 731–742.
- Tahvanainen, H., Pätynen, J., and Lokki, T. (2015b). "Studies on the perception of bass in four concert halls," *Psychomusicol.: Music Mind Brain* **25**(3), 294–305.
- Takahashi, D. (1997). "Seat dip effect: The phenomena and mechanism," *J. Acoust. Soc. Am.* **102**(3), 1326–1334.
- Twersky, V. (1957). "On scattering and reflection of sound by rough surfaces," *J. Acoust. Soc. Am.* **29**(2), 209–225.
- Webb, C., and Bilbao, S. (2011). "Computing room acoustics with CUDA-3D FDTD schemes with boundary losses and viscosity," in *IEEE International Conference on Acoustics, Speech and Signal Processing (ICASSP)*, pp. 317–320.
- Witew, I. B., Vorländer, M., and Xiang, N. (2017). "Sampling the sound field in auditoria using large natural-scale array measurements," *J. Acoust. Soc. Am.* **141**(3), EL300–EL306.